Construction and Building Materials 328 (2022) 127054

Contents lists available at ScienceDirect

Construction and Building Materials

journal homepage: www.elsevier.com/locate/conbuildmat

Evaluation of the shear and permanent deformation properties of cold in-place recycled mixtures with bitumen emulsion using triaxial tests

P. Orosa *, I. Pérez, A.R. Pasandín

Universidade da Coruña, Department of Civil Engineering, E. T. S. I. Caminos, Canales y Puertos, Campus de Elviña s/n, 15071, A Coruña, Spain

ARTICLE INFO

Keywords:
Cold in-place recycling
Bitumen stabilized material
Reclaimed asphalt pavement
Bitumen emulsion
Gyratory compactor
Triaxial testing
Shear properties
Permanent deformation
Rutting
Prediction model

ABSTRACT

The cold in-place recycling (CIR) technique is a road rehabilitation method suitable for a circular economy. Triaxial tests have proven to be suitable for studying the mechanical behaviour of cold mixtures. In this study, CIR specimens were prepared using a gyratory compactor with different proportions of bitumen emulsion. The Mohr–Coulomb diagrams and shear parameters were obtained by conducting monotonic triaxial tests at different confining pressures. The binder content provided adequate cohesion; however, an excess of binder reduced internal friction. Subsequently, repeated load permanent deformation triaxial tests were performed. Accordingly, critical stress ratios between 20% and 30% were obtained, and the mix with a 2.50% binder exhibited the best response. Lastly, two permanent deformation prediction models were fitted to the measured results. For high deformations, the Paute model underestimated the deformations, whereas the Huurman model demonstrated the best fit.

1. Introduction

Road and highway pavements are designed for a certain service life. Such infrastructures often require maintenance work or even major reconstruction because the materials experience fatigue or cracking, and may accumulate excessive permanent deformation from traffic flow, causing rutting [1]. Recently, cold recycling with bituminous emulsions has been one of the most widely used and studied techniques [2–4], which conforms with the circular economy and is sustainable for the environment. The solid phase used in these mixes is composed totally or in major part of reclaimed asphalt pavement (RAP), originating from the milling of worn roads, and the binder used is in the form of an emulsion or foamed bitumen; therefore, heating is not required. These characteristics mitigate the need for virgin aggregates and increase the likelihood of performing all operations at ambient temperature. Besides saving fossil fuel costs, the operating temperature also results in better working conditions for operators and the environment owing to the associated reduction in greenhouse gas emissions [5–7]. These cold recycled mixtures (CRMs) can be produced either in plant, by using specialised equipment, or on site, by cold in-place recycling (CIR). This recycling technique avoids the need for the transportation of large quantities of RAP to landfills, allowing it to be used in new mixtures after milling.

Prior to the field execution of a CRM, a laboratory study is usually conducted to enhance the design of the mixes. Typically, most design methods are based on the results of simple and quick tests, such as ITS, Marshall stability, UCS, and CBR, which provide empirical references that provide an approximate idea of the material characteristics [8]. The approach has been criticised by many experts and specialists in the road sector, who have attempted to introduce more feasible tests [9–11] that would subject the mixes to realistic tensional scenarios, similar to those they are likely to be exposed to in the field, and combine the results with predictive models, pavement design, and finite element method (FEM) software to estimate pavement response [12,13].

Despite being more complex and time-consuming, triaxial tests have proven their efficacy and adequateness for the study of this type of material. Triaxial tests allow to simulate the influence of the surrounding material through the application of different confining pressures to the tested mixtures and deviator stresses following different loading patterns. Hence, there are several possibilities for testing, from

Abbreviations: CIR, Cold In-Place Recycling; BSM, Bitumen Stabilized Material; CRM, Cold Recycled Mixture; RAP, Reclaimed Asphalt Pavement; ITS, Indirect Tensile Strenght; UCS, Unconfined Compressive Strenght; CBR, California Bearing Ratio; FEM, Finite Element Method; ME, Mechanistic-Empirical; SR, Stress Ratio; RLPD, Repeated Load Permanent Deformation; BC, Binder Content; AWC, Added Water Content; OFC, Optimum Fluid Content.

* Corresponding author.
E-mail addresses: p.orosa@udc.es (P. Orosa), iperez@udc.es (I. Pérez), arodriguezpa@udc.es (A.R. Pasandín).

https://doi.org/10.1016/j.conbuildmat.2022.127054
Received 23 November 2021; Received in revised form 21 January 2022; Accepted 2 March 2022
Available online 9 March 2022

monotonic triaxial tests to obtain the shear parameters to cyclic loading triaxial tests, which evaluates the resilient modulus using short-term tests, or the permanent deformation in tests with higher load cycles [14].

Following the preparation of CRMs, there are two clearly differentiated phases in their mechanical behaviour through their lifecycle [9–11]. First, in the curing phase, the mixtures evaporate the internal water, and is characterised by an increment in the strength capacity and stiffness. In this first phase, there is a clear nonlinear elastic behaviour similar to that of granular materials, which is stress-dependent. Following the curing phase, there is a second phase that involves a certain reduction in stiffness owing to aging and traffic loads. In this second phase, the behaviour becomes increasingly viscoelastic, and is characterised by a dependence on temperature and loading frequency, resembling a traditional hot mix. Therefore, the behaviour of CRMs is intermediate between a hot mix and a granular material, and the analysis using triaxial tests is considered adequate, particularly when the binder content is low, presenting predominantly granular behaviour with a stress-dependent response [9,15].

In previous research, authors conducted numerous cyclic loading triaxial tests on CIR mixtures to evaluate the short-term evolution of the resilient modulus and curing time [16]. Successive tests were performed under laboratory conditions without accelerated curing, and the correlation between the increment in stiffness and water loss with the curing period was observed. Moreover, the stress–dependent behaviour characteristic of granular materials without binder was also verified, enabling the fitting of popular predictive numerical models of the resilient modulus. In the present study, the same recycled mixtures were further examined by performing monotonic triaxial tests and subsequent long-term cyclic triaxial tests. The shear parameters and permanent deformation were studied by varying the proportions of binder and water used. Lastly, based on the results, it was possible to adjust mechanistic–empirical (ME) models to predict the permanent deformation of the studied CIR mixtures.

1.1. *Permanent deformation prediction models of granular materials used in road pavements*

Recoverable (elastic) or non-recoverable (plastic or permanent) deformations occur when the road surface is subjected to cyclic loads owing to the traffic that passes over it during its service life. Non-recoverable deformations are responsible for the appearance of rutting, which causes a deterioration of the road surface and discomfort for users [1]. Therefore, predicting and quantifying this deformation at the design stage are crucial to reduce the deformation as much as possible and plan appropriate maintenance work. Accordingly, since the 1950s, considerable efforts have been devoted to develop models for the prediction of the permanent deformation of unbound granular materials [17,18]. While the models for the resilient modulus are usually nonlinear equations dependent on the stress level, the prediction of permanent deformation is more complex and also depends on the number of load cycles applied.

Complex elastoplastic models can be used to assess the behaviour of materials subjected to a large number of cyclic loads. These models consider both permanent and elastic deformations. Despite their accuracy, they are difficult to implement and are computationally intensive [19]. Therefore, the conventional practice is to employ ME models that are fed with results from numerous laboratory tests, which allow the adjustment of different parameters, or to use models based on the Shakedown theory [20]. These models can predict the behaviour effectively and are much easier to implement than elastoplastic models.

The Shakedown theory is another approach for describing the response of a material to permanent deformation after long loading cycles. Accordingly, there is a certain load threshold (Shakedown limit) below which the material undergoes permanent deformation for a limited number of load cycles initially, after which it stabilises and behaves elastically. For load levels above the Shakedown limit, the material deforms plastically without stabilising, eventually causing failure. The Shakedown theory was developed by Werkmeister et al. [21] for granular materials without binder and was also detailed in standard EN 13286-7 [22]. According to this criterion, materials can be classified into three types depending on the applied load level (Fig. 1):

- Range A, also known as "Plastic Shakedown", occurs when the cumulative permanent deformation rate (ε_p / N) decreases rapidly until it stabilizes. From this equilibrium state, the deformation is elastic and does not produce permanent deformations. Therefore, the material does not reach failure.
- Range B, also known as "Plastic creep limit", occurs when the cumulative permanent deformation rate is decreasing or remains constant without stabilizing. The deformation is not completely elastic, and the material is susceptible to failure for a sufficiently large number of load cycles.
- Range C, also known as "Progressive plastic collapse", occurs when the cumulative permanent deformation rate increases rapidly, and failure occurs for a relatively small number of load cycles.

Approaches for road pavements based on this theory seek to find the shakedown limit to ensure that the service loading to which these materials are subjected to in the pavement will be lower, thus ensuring that there are no excessive deformations [23,24].

Finally, the ME prediction models are based on the results of laboratory tests, which are mostly triaxial tests. Traditionally, ME prediction models have been used in soil mechanics, and the choice of the most suitable one depends on the analysed material. In our case, the models used in road pavements are those used for granular materials; therefore, the focus will only be on those models, and not on models for sands or other cohesive soils. The preliminary models employed were based on power equations ($\varepsilon_p = a \cdot N^b$), only dependent on the number of loading cycles (N) and parameters of the material (a, b), capable of estimating the deformation of Range A and B materials, but could not predict the deformation reached by Range C materials, which after a certain number of cycles significantly increased the strain rate until collapse. Generally, the material parameters are fitted by regression from a series of triaxial tests [25,27,29–31]. Additional models of higher complexity were subsequently developed, which considers temperature, loading time, resilient modulus, or the stress state, by including different factors, such as the deviatoric stress $q = \sigma_d = \sigma_1 - \sigma_3$, the mean stress $p = (\sigma_1 + 2\sigma_3)/3$, the stress ratio of the deviator stress expressed as $SR = q/q_f = \sigma_d/\sigma_{d,f}$, or even the shear parameters (internal friction angle and cohesion) [25,27,31–33]. Some of the most popular permanent deformation prediction models for granular material used for cold mixtures in road engineering are summarized in Table 1.

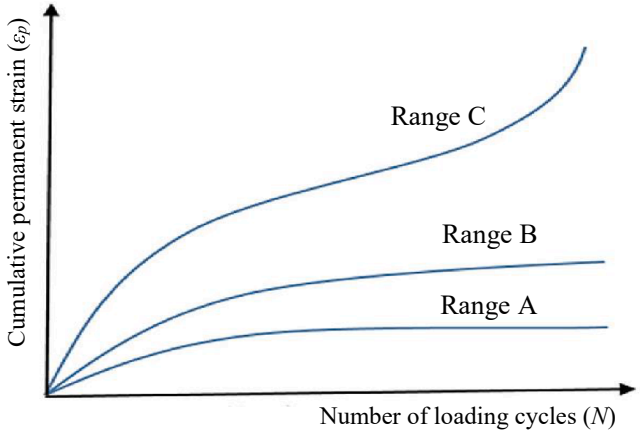

Fig. 1. Shakedown theory diagram.

Table 1
Mechanical-empirical models of permanent deformation employed on road pavements.

Authors	Permanent deformation models	Parameters
Barksdale (1972) [25]	$\varepsilon_p = a \cdot b\log(N)$	a, b denote regression parameters
	$\varepsilon_p = \frac{\frac{q}{a \cdot \sigma_3^b}}{1 - \left[\frac{SR \cdot q \cdot (1 - \sin\varphi)}{2(C \cdot \cos\varphi + \sigma_3 \cdot \sin\varphi)}\right]}$	"a. σ_3b" denotes a relationship defining the initial tangent modulus as a function of σ_3 SR indicates the stress ratio ($SR = q/q_f = \sigma_d/\ \sigma_{d,f}$) φ denotes the internal friction angle and C represents the cohesion
Francken (1977) [26]	$\varepsilon_p = A \cdot \left[\left(\frac{N}{1000}\right)^B\right] + C \cdot \left(e^{D \cdot \frac{N}{1000}} - 1\right)$	A, B, C, D denote the regression parameters
Paute et al. (1988, 1994) [27,28]	$\varepsilon_p = A \cdot N^B + C$	A, B, and C are regression parameters
	$\varepsilon_p = \varepsilon_p(100) + f(N) \cdot A$ $f(N) = 1 - \left(\frac{N}{100}\right)^{-B}$ $A = \frac{\frac{q}{p + p^*}}{a - b \cdot \frac{q}{p + p^*}}$	ε_p *(1 0 0)* is the permanent deformation after the first 100 cycles A can be obtained as a regression parameter or using the stress-dependent expression B, a, and b are regression parameters $p^* = m / s$, where $q = m \cdot p + s$ is the failure equation of the material
Sweere (1990) [29]	$\varepsilon_p = a \cdot N^b$ $L(\varepsilon_p) = a + b \cdot L(N)$	a, b are regression parameters
Vuong (1994) [30]	$\varepsilon_p = \varepsilon_r \cdot \left(\frac{a}{b}\right) \cdot N^c$	a, b, c are regression parameters ε_r is the resilient deformation
Wolff and Vissier (1994) [31]	$\varepsilon_p = (c \cdot N + a)(1 - e^{-bN})$	a, b, c are regression parameters
Lekarp and Dawson (1998) [32,33]	$\frac{\varepsilon_p(N_{ref})}{L/p_0} = a \cdot \left(\frac{q}{p}\right)^b_{max}$	a, b are regression parameters N_{ref} $L = \sqrt{q^2 + p^2}$ $p_0 = 100$ kPa (reference mean stress)

2. Aims and scope

In this study, monotonic and repeated load permanent deformation (RLPD) triaxial tests were performed on CIR mixtures with different binder proportions to expand the current knowledge on the mechanical behaviour of CRMs. Cylindrical specimens were prepared with a gyratory compactor using three different bituminous emulsion contents, corresponding to residual binder contents of 2.00%, 2.50%, and 3.00%, while maintaining a constant optimum fluid content. Thus, it was possible to evaluate the influence of different dosages on the studied behaviour.

Monotonic triaxial tests were performed on the uncured and cured specimens (72 h in an oven at 50 °C) to evaluate the impact of curing. Four different confining pressures were used (25, 50, 100, and 200 kPa) to determine the lines of failure and shear parameters (cohesion and internal friction angle) in each case. From the failure lines, it was possible to perform RLPD triaxial tests at different percentages of the failure load (i.e., at different stress ratios), investigating the evolution of the permanent deformation up to 90,000 load cycles for each mix and stress level. Besides, two ME prediction models of permanent deformation were fitted based on the measured results, obtaining the characteristic parameters of the studied mixtures, and the goodness-of-fit was analysed in each case.

3. Materials and manufacturing

3.1. Materials

The solid phase of the specimens prepared in this study consisted entirely of RAP, which was provided by a local quarry near the city of A Coruña (Spain). Fig. 2 shows the black gradation of RAP obtained according to EN 12697–2 [38]. Combined with the RAP grain sizes, Fig. 2 includes the gradation limits recommended for CIR with bituminous emulsion from the Spanish specification PG-4 [39], as well as those from the South African BSM guide TG2 [40].

A slow-setting cationic emulsion with 60% binder content (BC) was used, named C60B5–REC, in accordance with the European nomenclature specified in the standard EN 13,808 [41], which is commonly used in CIR. Table 2 summarises the main characteristics of the RAP and its recovered bitumen, and those of the emulsion and bitumen used in its production.

3.2. Mix design

In accordance with the current Spanish PG-4 specification for the design of CIR mixes [39], the calculation of the proportions of bitumen emulsion and added water used were based on the optimum fluid content (*OFC*) resulting from the modified Proctor test (MPT) [47]. To maintain the *OFC*, Equation (1) included in PG-4 [39] was used to determine the added water content (*AWC*) for the different *BCs* considered.

$$AWC(\%) = OFC(\%) - 0.5\ \% - BC(\%) \quad (1)$$

The *OFC* obtained from the MPT was 5.75%. According to previous experiences with the same RAP [8,16], the binder and water contents used in the three mixtures studied are listed in Table 3, together with their equivalent emulsion contents (EC).

3.3. Specimen preparation

An automatic mixer was used to prepare all mixtures studied. The mixing procedure involves two phases. First, the RAP was mixed with the corresponding AWC for 60 s. The emulsion was then added and mixed for 90 s. Once the mixtures were prepared, the compaction was performed using a gyratory compactor according to the standard EN 12697–31 [48]. The gyratory compaction parameters were as follows: an internal rotation angle of 0.82°, rotatory speed of 30 rpm, and 600 kPa of compaction pressure. The specimens were compacted such that the contents of air voids (V_a) in all specimens were the same. This was possible by compacting in each case to the desired density, based on the maximum specific gravities (ρ_m) previously calculated according to EN 12697–5 [49] (Table 3). Since the V_a is one of the most influential parameters in the stiffness and shear behaviour of the mixes [50], fixing it allowed the determination of the influence of the binder content between two mixtures. Thus, based on a previous study on the compaction of these CIR mixtures [51], the compaction was performed with a standard number of gyrations between 100 and 130 [39], so that the V_a of the cured specimens was fixed at 18.0 ± 0.3%. The purpose of ensuring the same V_a for all specimens was to facilitate the study of the influence of the dosage of each mixture on the results obtained.

In accordance with EN 13286-7 [22], the height of triaxial specimens must be twice the diameter. Therefore, as in previous experiences with this test [16], specimens were manufactured by stacking two specimens of 100 mm height and 100 mm diameter, successively compacted, one on top of the other, yielding specimens with a height of 200 mm. This fabrication method has been adopted by other scholars [14,52–54], and

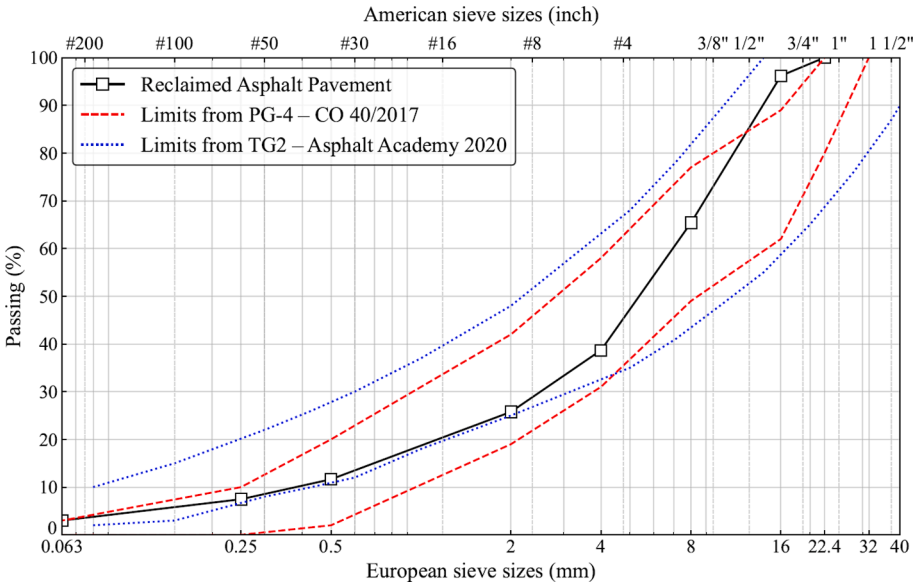

Fig. 2. RAP gradation compared with limits in PG-4 and TG2 specifications.

Table 2
Properties of RAP and bitumen emulsion.

RAP and recovered bitumen	Standard	Unit	Value
Binder content	NLT-164/90 [42]	%	4.45
Nominal maximum particle dimension	EN 12697–2 [38]	mm	22.4
Maximum specific gravity	EN 1097–6 [43]	kg/m^3	2425
Softening point	EN 1427 [44]	°C	70.2
Penetration (25 °C)	EN 1426 [45]	dmm	32.15
Bitumen emulsion and residual binder			
Residue content (bitumen)	EN 1429 [46]	%	60
Softening point	EN 1427 [44]	°C	36.5
Penetration (25 °C)	EN 1426 [45]	dmm	170

Table 3
Proportions of binder and water used, and maximum densities of the studied mixtures.

Mixtures	BC (%)	EC (%)	AWC (%)	OFC (%)	ρ_m (kg/m^3)
2B_3.25W	2.00	3.33	3.25	5.75	2431.51
2.5B_2.75W	2.50	4.17	2.75	5.75	2404.21
3B_2.25W	3.00	5.00	2.25	5.75	2394.60

the resulting triaxial specimens behaved as a single specimen when tested under principal axis stresses.

In this study, specimens subjected to accelerated curing and uncured specimens were tested. Accelerated curing was performed in an oven at 50 °C for 72 h, until a constant weight of the specimens was reached. The specimens that were tested without curing were maintained at room temperature under laboratory conditions for 4 h after preparation. Subsequently, the uncured specimens were subjected to the tests. The objective of testing the uncured specimens was to simulate the behaviour of a CIR immediately following its on-site implementation. The same procedure for triaxial testing of uncured specimens was followed in the study of the evolution of the resilient modulus of the same mixtures in the short term [16]. Importantly, at younger ages after compaction, the specimens must be manipulated with special caution to avoid any damage to the specimens.

4. Methods

Triaxial tests were employed to assess the shear behaviour and permanent deformation response. During the triaxial tests, the specimens were stressed in three perpendicular directions. The major principal stress (σ_1) was applied in the direction of the specimen axis, perpendicular to the bases, simulating the vertical stress caused by the passage of a vehicle on the road. The lower principal stress (σ_3) or confining stress was applied perpendicular to the sides of the specimen, simulating the resistance exerted by the adjacent material within the pavement layers, opposing the generated deformations.

The triaxial equipment used for these tests comprised a removable sealed chamber and a vertical pneumatic press capable of handling the axial load (Fig. 3b). An air compression system was also utilized to apply a confining pressure inside the chamber (up to 10 bar). It was possible to register axial deformations using two linear variable deformation transducers (LVDT) positioned on the upper plate of the chamber (Fig. 3b).

The specimens were isolated by placing them inside an elastic rubber membrane that was connected to porous plates at the top and bottom using O-rings (Fig. 3a). Thus, pressurised air was prevented from entering the membrane, thereby achieving effective confinement of the specimens during the test. All triaxial tests performed in this investigation were performed under laboratory conditions (temperature, 22 ± 2 °C; relative humidity, 50 ± 5%).

4.1. Shear strength assessment

4.1.1. Monotonic triaxial testing

The shear strength of the CIR mixtures was studied by performing monotonic triaxial tests until failure with a constant confining pressure (CCP). In each case, the tests commenced from a state of tensional equilibrium ($\sigma_1 = \sigma_2 = \sigma_3$), and the deviatoric stress σ_d, was increased until the failure of the specimen. The rate of increase of σ_d was constant at 2.60% strain per minute (because all specimens were 200 mm in height, this strain was equivalent to 5.30 mm/min) until fracture occurred. For each mix, four different confining pressures, σ_3, were used (25, 50, 100, and 200 kPa) to obtain four associated principal and deviatoric stresses of failure ($\sigma_{1,f}$ and $\sigma_{d,f}$), resulting in four points of the Mohr–Coulomb failure envelope. Figure 4 illustrates a schematic of the results of a CCP monotonic triaxial test performed on one of the tested specimens. Monotonic triaxial tests were performed on the three studied mixtures (Table 3), for both cured and uncured cases, and six failure lines were obtained.

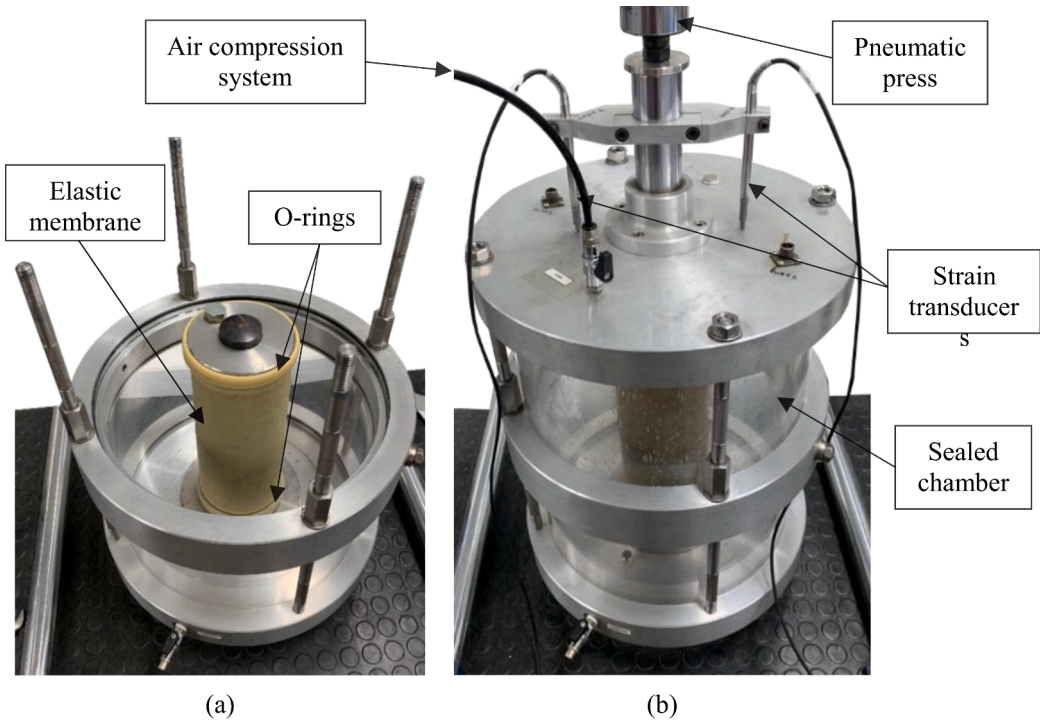

Fig. 3. Details of the sealed triaxial chamber, containing a specimen previously to be tested: (a) chamber disassembled to facilitate placement of the specimen; (b) chamber closed and ready to start the triaxial test.

4.1.2. Mohr–Coulomb failure criterion

The Mohr–Coulomb failure criterion is used extensively in soil mechanics. Since CIR mixtures have a similar composition to that of granular materials, with stress-dependent behaviour, such asphalt mixtures can be modelled as Mohr–Coulomb materials with cohesive properties.

The Mohr–Coulomb circle was constructed from the major and minor principal stresses of the specimen at failure ($\sigma_{1,f}$ and σ_3, respectively), with $(\sigma_{1,f}+\sigma_3)/2$ being the centre of the circle and $(\sigma_{1,f}-\sigma_3)/2$ being the radius (Fig. 4). When at least three Mohr circles are plotted (each of which corresponds to a different value of the confining stress), a tangent to these circles, known as the failure envelope, can be plotted (Fig. 4). Any combination of principal and shear stresses above the line causes failure of the test specimen and therefore of the pavement layer constructed with the studied material. The Mohr–Coulomb failure-line equation can be expressed mathematically using Equation (2).

$$\tau_{ff} = tan\varphi \cdot \sigma_{ff} + C \quad (2)$$

where τ_{ff} and σ_{ff} represent the shear and normal stresses when failure occurs, respectively, C denotes the cohesion of the material, and φ denotes the internal friction angle.

Furthermore, the maximum principal and maximum deviatoric stresses resisted by the specimen at the time of collapse, $\sigma_{1,f}$ and $\sigma_{d,f}$, are linear functions of the confining pressure σ_3 [10,55], and their relationships are described in Equations (3)–(5).

$$\sigma_{1,f} = A \cdot \sigma_3 + B \quad (3)$$

$$A = (1 + sin\varphi)/(1 - sin\varphi) \quad (4)$$

$$B = (2C \cdot cos\varphi)/(1 - sin\varphi) \quad (5)$$

From the experimental results of the monotonic triaxial tests (σ_3, $\sigma_{1,f}$), it was possible to determine parameters A and B using a linear regression. Subsequently, C and φ were calculated for each mix.

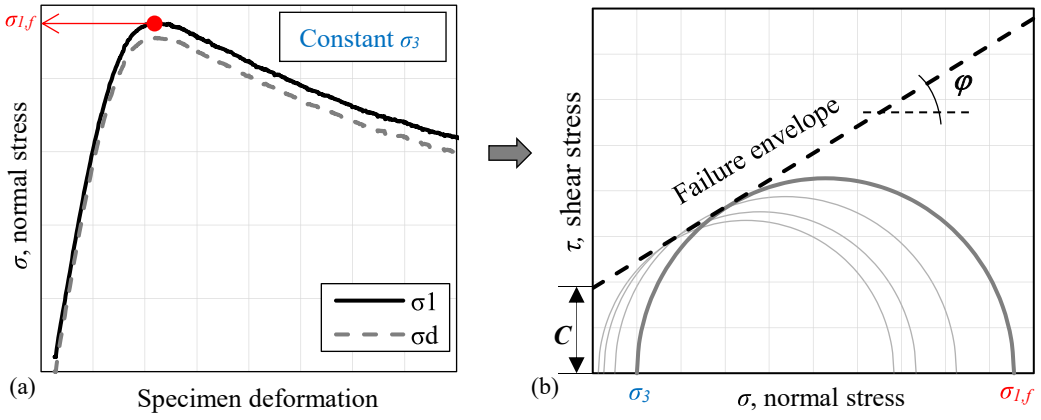

Fig. 4. (a) Scheme of a monotonic triaxial test result with a constant σ_3; (b) Mohr–Coulomb circle plotted from the result of the test.

4.2. Permanent deformation response

4.2.1. Dynamic triaxial testing

The permanent deformation behaviour of the CIR mixtures was studied according to standard EN 13286-7 [22] using RLPD triaxial tests with CCP and sinusoidal variation of σ_d (Fig. 5a). The specimens were manufactured in the same method as those previously used in monotonic triaxial tests, with a height of 200 mm and diameter of 100 mm, and placed inside a sealing membrane.

In accordance with the followed standard [22], the testing commenced with the application of an initial σ_3 of 20 kPa and σ_d of 5 kPa (the latter was chosen to be greater than 0 to ensure continuous contact between the specimen and actuator). Subsequently, σ_d was applied for up to 90,000 load cycles, recording the deformation of 10 consecutive cycles when the following numbers of cycles were completed: 1, 10, 50, 100, 200, 400, 1000, 2500, 5000, 7500, 10000, 12500, 15000, 20000, 30000, 40000, 50000, 60000, 70000, 80000, and 90000.

A CCP of 50 kPa was used for all RLPD triaxial tests. For each mix examined, tests were repeated for different specimens using different stress ratios, determined as $SR = \sigma_d/\sigma_{d,f}$, where $\sigma_{d,f} = \sigma_{1,f} - \sigma_3$. For each mix, the respective $\sigma_{d,f}$ values were obtained from the failure envelopes derived from monotonic triaxial tests. Fig. 5b illustrates the typical relationship between the number of load cycles and the permanent deformation resulting from tests of this type. The permanent deformation response curve is divided into three stages or zones: primary (or transient), secondary (or steady-state), and tertiary. The cycle number at which the tertiary stage commences is known as flow number (F_N). Six different *SRs* were used (20%, 30%, 40%, 50%, 60%, and 80%) to demonstrate the difference between curves that completed the 90,000 cycles with a deformation that tended to stabilise and curves that reached the tertiary flow stage (Fig. 5b). Thus, it was possible to determine the critical *SR* value at which the tertiary flow stage was reached before 90,000 cycles in each mixture. Once tertiary flow was achieved, the slope of the deformation curve increased rapidly until failure of the specimen without completing the examined number of cycles.

4.3. Computational modelling of permanent deformation behaviour

Based on the results obtained in the RLPD triaxial tests, two of the predictive models of permanent deformation from Table 1 were used for fitting. Most of the models listed in Table 1 are only dependent on the number of load cycles (*N*), and their parameters must be adjusted for each stress state considered. Pérez et al. [56,57] successfully fitted this type of simple models when studying the permanent deformation of granular materials in roads. Moreover, other authors have also fitted similar models to predict the permanent deformation of bitumen stabilised materials (BSM), as a function of *N* and also the stress state [10,14,59]. In the present study, the selected models also included the dependence on the existing stress level, obtaining regression parameters that are characteristic of the material and independent of the stress state. In each case, the goodness of fit of each model was also compared to determine the model that best predicted the measured permanent deformation.

The first of the fitted models was the model proposed in 1994 by Paute, Hornych, and Benaben [28], known as Paute's model, or Hornych's model (6), depending on the literature consulted. The model predicts the permanent deformation starting from the deformation measured at 100 loading cycles ε_p (1 0 0), as the product of a function of *N* (7) and a function of the stress state A (8), as shown below:

$$\varepsilon_p = \varepsilon_p(100) + f(N)\cdot A \tag{6}$$

$$f(N) = 1 - \left(\frac{N}{100}\right)^{-B} \tag{7}$$

$$A = \frac{\frac{q}{p+p^*}}{a - b\cdot\frac{q}{p+p^*}} \tag{8}$$

where a, b, and B denote the only regression parameters, q and p represent the deviatoric and mean stresses, respectively, and $p^* = m/s$, where $q = m\cdot p + s$ corresponds to the failure equation of the material in terms of p and q.

The second model was proposed by Huurman [35], which is a variation of the Francken model (9), in which the regression parameters are a function of the stress level in terms of σ_d and *SR*, as described in Eqs. (10)–(13), independent of the confining pressure σ_3.

$$\varepsilon_p = A\cdot\left[\left(\frac{N}{1000}\right)^{B}\right] + C\cdot\left(e^{D\cdot\frac{N}{1000}} - 1\right) \tag{9}$$

$$A = a_1\cdot\left(\sigma_d/\sigma_{d,f}\right)^{a_2} \tag{10}$$

$$B = b_1\cdot\left(\sigma_d/\sigma_{d,f}\right)^{b_2} \tag{11}$$

$$C = c_1\cdot\left(\sigma_d/\sigma_{d,f}\right)^{c_2} \tag{12}$$

$$D = d_1\cdot\left(\sigma_d/\sigma_{d,f}\right)^{d_2} \tag{13}$$

where a_1, a_2, b_1, b_2, c_1, c_2, d_1, and d_2 denote the regression parameter characteristics of the material and ($\sigma_d/\sigma_{d,f}$) denotes the considered *SRs*. A particular feature of the Huurman model that differentiates it from the previous one and makes it particularly interesting is that the second summand is an exponential term, producing rapid growth in the

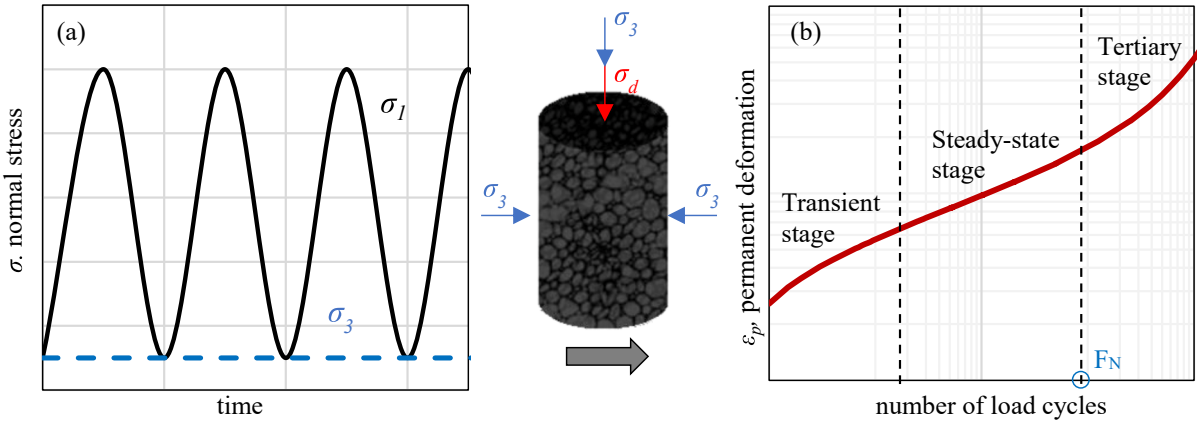

Fig. 5. Scheme of the stresses applied during an RLPD triaxial test, and the results obtained: (a) sinusoidal variation of the vertical stress and CCP; (b) shape of the cumulative permanent deformation curve.

predicted permanent deformations for high numbers of load cycles.

5. Results and discussion

5.1. Shear strength assessment

Monotonic triaxial tests were performed until the failure of the three studied CIR mixtures, cured and uncured, using four different confining pressures. For each confining pressure, σ_3, the normal principal stress at failure, $\sigma_{1,f}$, was obtained. These pairs of points are shown in the plots of Fig. 6a and 6b. It was also possible to plot the *p*–*q* diagrams, which are represented in the plots of Fig. 6c and 6d. Linear regressions were performed to establish the stress relationships in each case for the three mixes, both cured and uncured.

Because all the mixtures were manufactured with a similar air void content (Table 4), and since the *OFC* was kept constant in all of them (Table 3), it is worth noting that the differences shown in their shear behaviour results were primarily owing to the different *BCs* used. Thus, the first result highlighted in Fig. 6 is that the results for the uncured mixtures are very similar in all three cases. It was because at such early ages, the water in the mixture had not yet evaporated and the binder in the emulsion had not yet developed its cohesive function. As for the results after 3 d of curing at 50 °C, a general increase in $\sigma_{1,f}$ values was observed for the same σ_3 compared to the uncured case, as observed when comparing the plots in Fig. 6. The highest increment was observed in the mix with 2.00% *BC*, which increased its $\sigma_{1,f}$ by 61.13% for σ_3 of 200 kPa, whereas the mixes with 2.50% and 3.00% *BC* increased it by 21.84% and 28.31%, respectively. Furthermore, also the mix with the lowest *BC* exhibited the highest slope in the linear regression. This result was caused by the greater influence of its mineral skeleton, which also led to a greater angle of internal friction (Table 4), revealing the major significant stress–dependent behaviour of the CIR when the binder content was reduced.

Table 4
Shear parameters and air void contents of the studied mixtures.

Mixture	V_a (%)	C (kPa)	φ (°)	R^2
2B_3.25W. cured	18.29	364.82	42.70	90.06%
2B_3.25W. uncured	15.05	167.07	40.24	99.50%
2.5B_2.75W. cured	17.82	373.60	30.60	99.01%
2.5B_2.75W. uncured	15.03	176.93	38.38	99.13%
3B_2.25W. cured	17.79	426.52	27.05	96.63%
3B_2.25W. uncured	15.15	187.23	36.58	95.33%

The relationships established between σ_3 and $\sigma_{1,f}$, obtained from the results of the monotonic triaxial tests (Fig. 6) also enabled the calculation of parameters *A* and *B* (3) and determination of the Mohr–Coulomb diagrams. Hence, for each mixture, both uncured and cured four different Mohr–Coulomb circles were plotted (one for each confining

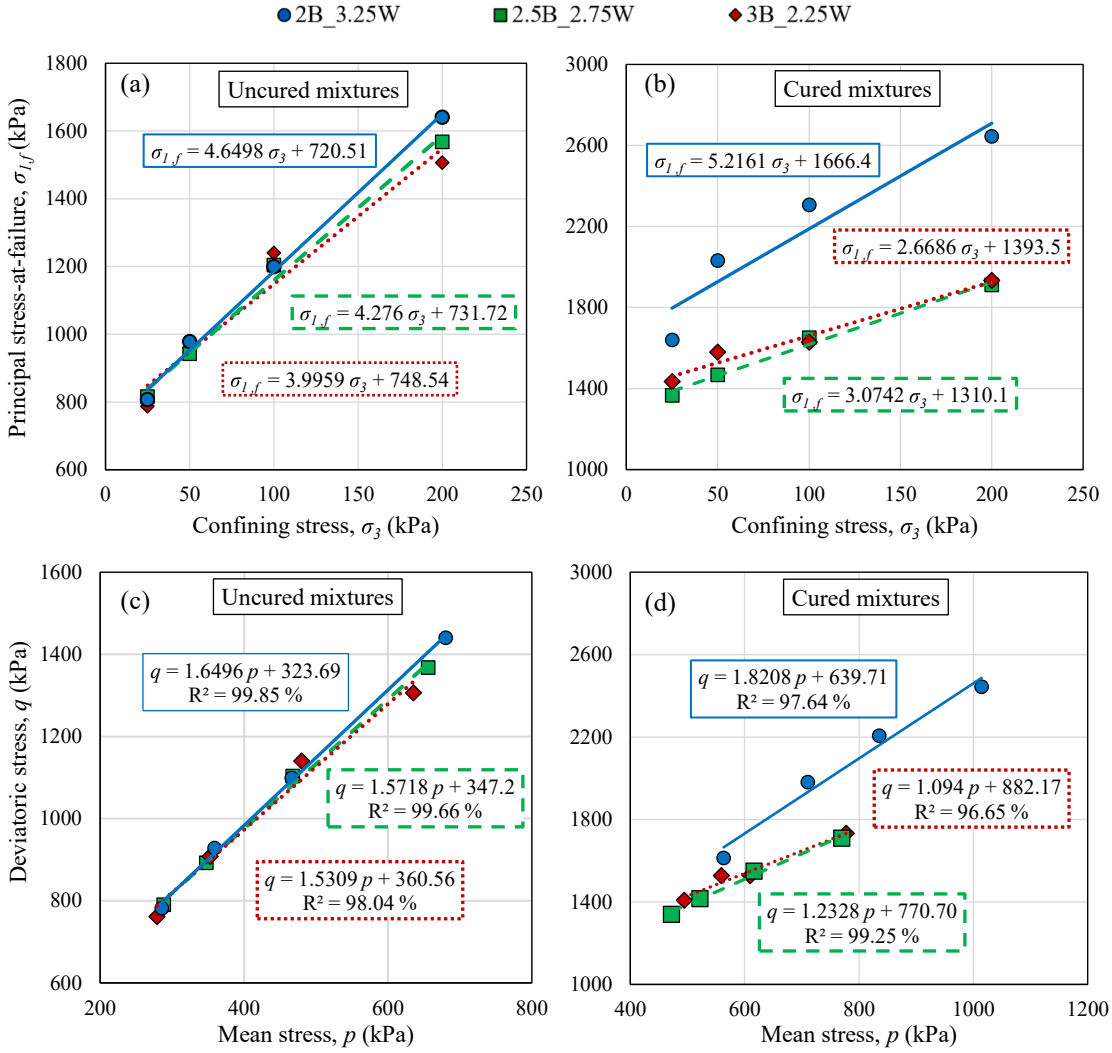

Fig. 6. Stress relationships for the studied uncured and cured CIR mixtures: (a and b) between the major principal stress at failure, $\sigma_{1,f}$, and the confining stress, σ_3; (c and d) p–q diagrams.

stress), as shown in Fig. 7.

Collectively, the Mohr–Coulomb diagrams and Equations (2) to (5) were used to obtain the shear parameters, C and φ, as well as the failure envelopes for each of the cured and uncured mixtures. The six different failure envelopes are also plotted tangentially to the respective Mohr–Coulomb circles in Fig. 7. These results are summarised in Table 4, together with the average air void content (V_a) in each case and the coefficients of determination, R^2.

The failure envelopes of the three mixes, uncured and cured, are plotted in Fig. 8 to better compare one mix with another. Again, it can be seen that the uncured mixes exhibited smaller differences, although the influence of the binder could already be perceived, albeit to a minor degree, in both Fig. 8a and Table 4. Hence, the cohesion results were slightly higher for the mixtures with higher *BCs*, whereas the opposite occurred with the internal friction angle, which was reduced. The difference was only 12.07% between the major and minor cohesion results and a 10% difference was observed in terms of the internal friction angle.

After curing, the binder in each mixture plays a fundamental role, and the differences between the mixtures become more noticeable. As expected, there was a considerable general increase in cohesion results (Table 4), with a more than twice increment in all cases. Thus, the cohesion values increased by 118.36%, 111.16%, and 127.81% for the mixtures with 2.00%, 2.50%, and 3.00% BC, respectively. However, the internal friction angle only increased in the mixture with the lowest BC by 6.11% and decreased by 20.27% to 26.05% in the other two cases. Other researchers have already reported the greater influence of the moisture content in the mixture on the cohesion than on the internal friction in the BSM [58,59]; hence, the main differences occurred in the cohesion results. A higher BC provided greater cohesion, while acting as a lubricant between the mineral skeletons and reducing friction. A similar conclusion for the BSM was also described by Jenkins [9].

The cured mixture with the lowest *BC* (i.e., 2.00%) exhibited the highest φ value, as predicted from the highest slope in the Fig. 8b. The φ of the cured mix 2B_3.25 W was 39.54% higher than that of mix 2.5B_2.75 W, and 57.86% higher than that of mix 3B_2.25 W. However, the opposite occurred in the cohesion results, and it was the mix with the highest *BC* (i.e., 3.00%) the one that exhibited the highest value of C. In this case, the cohesion of the cured mix 3B_2.25 W was 14.16% higher than that of mix 2.5B_2.75 W, and 16.91% higher than that of mix 2B_3.25 W. As expected, after the curing period, when the mixtures developed their properties, the C values increased more sharply with the increase in BC than for the uncured mixtures, which, however, led to a decrease in the internal friction between the aggregates.

It was concluded that for all the *BCs* used, there was a considerable increment in the C of all the studied mixtures after curing, obtaining

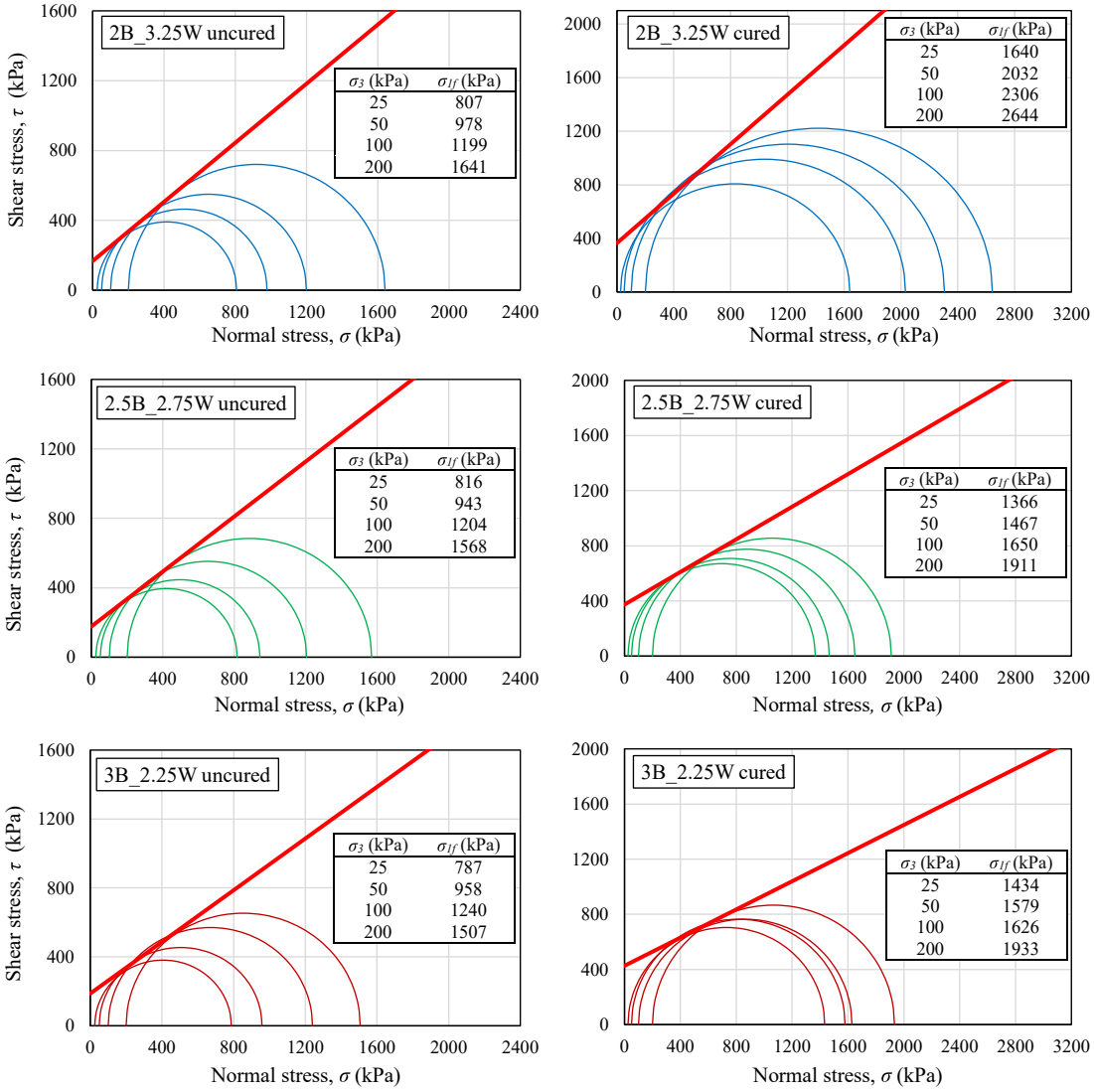

Fig. 7. Mohr–Coulomb diagrams for uncured and cured mixtures.

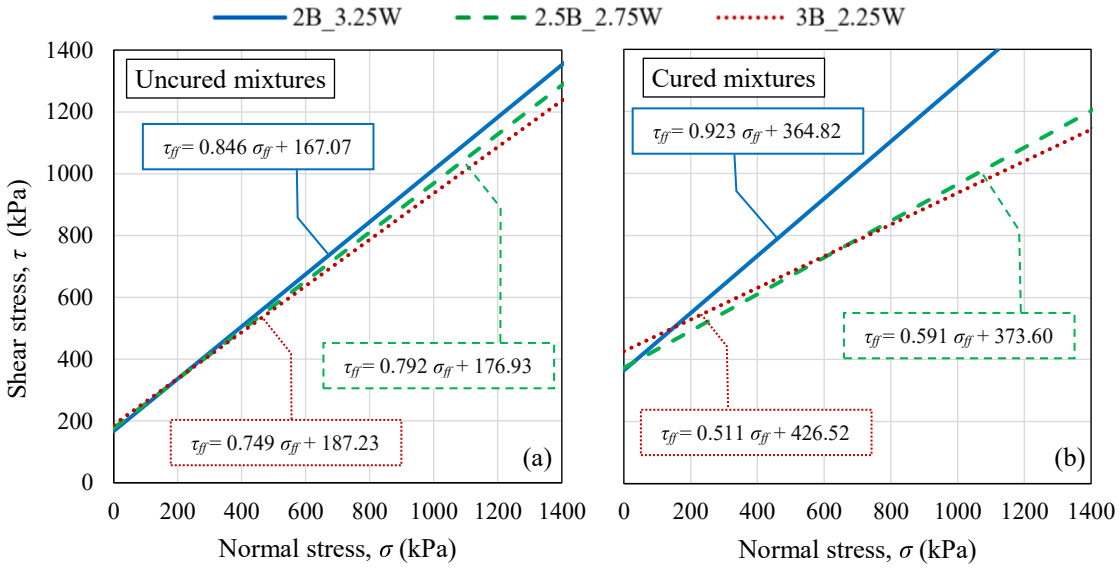

Fig. 8. Mohr–Coulomb failure envelopes corresponding to the studied mixtures: (a) uncured specimens; (b) specimens cured for 3 d at 50 °C.

values that were not significantly different. However, the φ results were more variable with dosage, and the highest φ was obtained for the mix with the lowest *BC*. Therefore, mixtures with higher *BC* values exhibited slightly higher cohesion. However, the influence of *BC* was the most noticeable in terms of internal friction. A higher *BC* led to a reduction in the internal friction owing to the side effect of lubrication between the aggregates.

Fig. 9 illustrates the typical shape of CIR specimens subjected to monotonic triaxial testing until failure. According to the soil mechanics theory, this failure plane angle is related to the internal friction angle (φ) through the expression$\Theta = 45 + \varphi/2$. From the images in Fig. 9, it can be seen that this approach was reasonably accurate because the failure plane was inclined at approximately 60°. The fact that the failure plane was continuous between the upper and lower specimens confirmed the correct behaviour of triaxial specimens manufactured by stacking two specimens when tested under vertical axis stresses, behaving as a single specimen.

5.2. Permanent deformation response

The stress relationships obtained in the previous section between σ_3 and $\sigma_{1,f}$ allowed the values of $\sigma_{1,f}$ and $\sigma_{d,f}$ to be obtained by fixing the value of σ_3 (Fig. 6). The RLPD triaxial tests were performed with a CCP $\sigma_3 = 50$ kPa on the cured mixtures, for which the corresponding values of $\sigma_{1,f}$ and $\sigma_{d,f}$ are listed in Table 5. Based on these values and according to the *SR* (σ_d / $\sigma_{d,f}$) considered for each test, deviatoric stresses were obtained.

For each of the three cured CIR mixtures, the results obtained from

Table 5
Major principal stress and deviator stress at failure for $\sigma_3 = 50$ kPa. Critical stress ratio, and applied deviator stress ($\sigma_{d,a}$) from which tertiary flow is produced before 90,000 cycles.

Mixture	σ_3 (kPa)	$\sigma_{1,f}$ (kPa)	$\sigma_{d,f}$ (kPa)	SR (%)	$\sigma_{d,a}$ (kPa)
2B_3.25W	50	1927	1877	30	563
2.5B_2.75W	50	1464	1414	30	424
3B_2.25W	50	1527	1477	20	295

Fig. 9. Shape of CIR specimens after monotonic triaxial test. Failure plane at approximately 60°.

the RLPD triaxial tests are presented in Fig. 10 for different *SRs*. The cumulative plastic deformations over the cycles are plotted on the left in Fig. 10a, 10b, and 10c, and are expressed in rates per thousand over the total height of the specimens. The cumulative permanent deformation rates (ε_p / N) versus the cumulative permanent deformations are plotted on the right in Fig. 10d, 10e, and 10f.

The critical *SRs* (Shakedown limits) from which the tertiary flow was produced before the 90,000 cycles were determined by analysing and comparing the evolution of the deformation curves in Fig. 10a to 10c with the number of load cycles, and the permanent deformation rates in Fig. 10d to 10f for each mixture. It can be observed in Fig. 10a to 10c that although the deformation curves started at different points, owing to the different deformations in the initial cycle, the slopes after reaching the second stage ("steady-state") became practically constant for each mixture, and the deformation rates were practically vertical lines. Upon reaching the tertiary stage, the deformation slopes increased rapidly again, and the deformation rates stopped decreasing. Thus, when the curves of the permanent deformation rates in Fig. 10d–10f were more vertical, the permanent deformations tended to stabilise (range A or B according to the Shakedown theory). In the case of the mixtures with 2.00% and 2.50% *BC*, for *SRs* of 20% and 30%, the lines were quite vertical and the permanent deformation rates decreased (Fig. 10d and 10e); therefore, the deformations tended to stabilise (Fig. 10a and 10b). However, for the remaining higher *SRs*, the

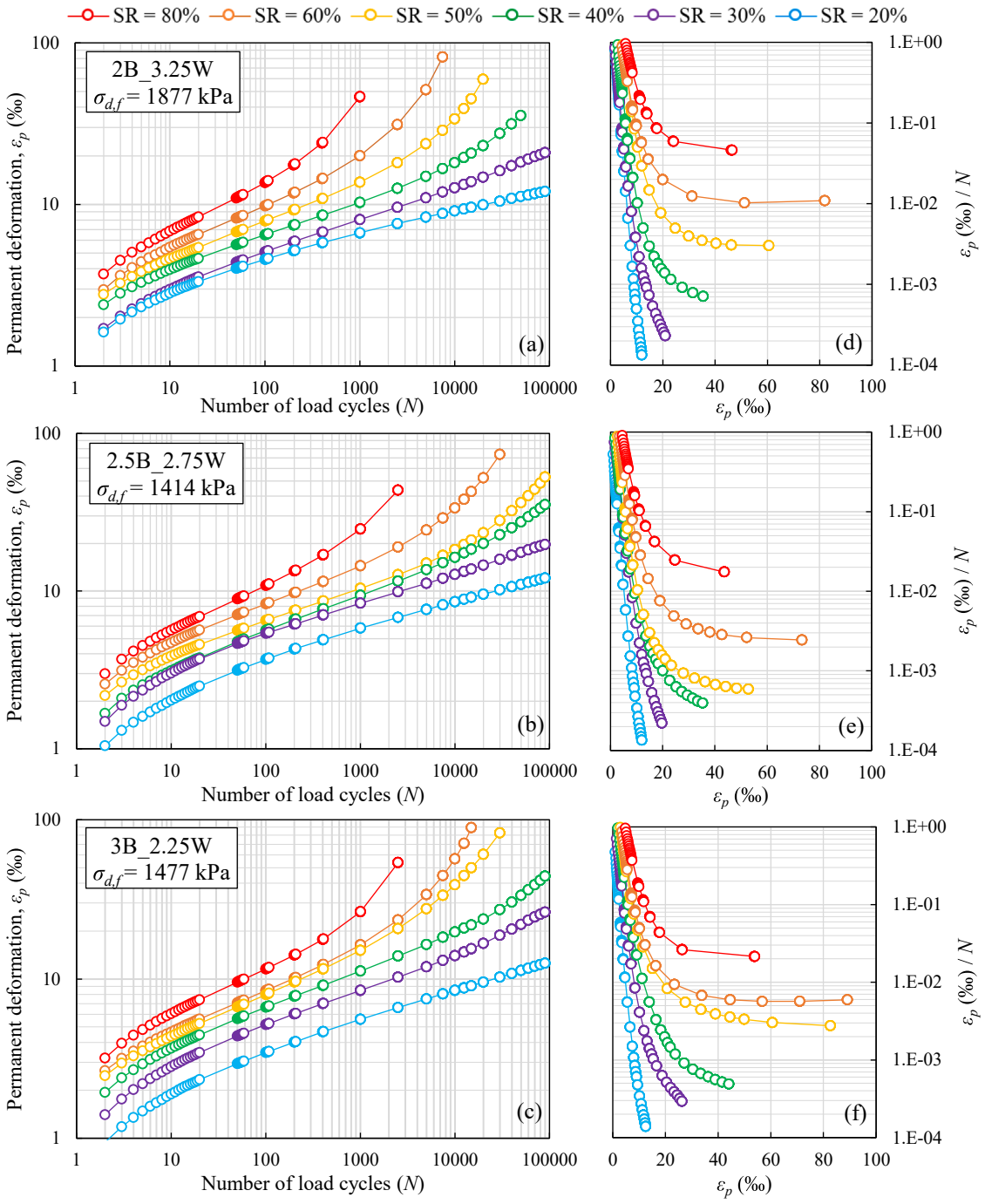

Fig. 10. Results of the RLPD triaxial tests of the three mixtures studied, after 3 d of curing at 50 °C at the different SRs considered: (a, b, and c) cumulative permanent deformation versus the number of load cycles; (d, e, and f) cumulative permanent deformation rate versus cumulative permanent deformation.

deformation rate lines were no longer vertical, indicating that the permanent deformation continued to increase without decreasing in the deformation rate. In these cases, there was no stabilisation of the deformations and the tertiary stage was reached (range C). The critical *SR* for mixes 2B_3.25 W and 2.5B_2.75 W was 30%. As for the mixture with 3.00% *BC*, Fig. 10f shows that only the line corresponding to 20% *SR* was vertical. Compared to the previous mixtures, the permanent deformation curve corresponding to *SR* = 30% in Fig. 10c and 10f did not exhibit a tendency to stabilise; therefore, the critical *SR* of the 2B_2.25 W mixture was considered to be 20%.

In each case, the critical *SRs* and the corresponding deviatoric stresses are summarised in Table 5. When there are stress levels above the critical *SR* in the CIR layer, failure by rutting of the pavement section is considered to occur. It was observed that for increasing *BCs*, the critical *SR* values tended to decrease in line with the decrease in the deviatoric stress at failure (in absolute terms). The critical *SR* results were lower than those obtained by other researchers in previous studies on the permanent deformation of BSM, obtaining values of *SR* ranging from 40% to 50% [9,10,14]. The worse permanent deformation behaviour could be related to the volumetric properties of the prepared mixtures, as compaction is known to be closely related to the shear and permanent deformation responses in BSM [59]. The studied mixtures exhibited some compactability difficulties [51], presenting a relatively high content of air voids compared to other studies on CIR; therefore, a weaker response to permanent deformation was expected.

The three mixtures are represented together in graphs corresponding to each of the *SRs* considered (Fig. 11) to facilitate a more accurate analysis of the response to permanent deformation of the mixtures. Moreover, two horizontal dotted lines indicating permanent deformations of 2.00% and 4.00% were added to each graph in Fig. 11.

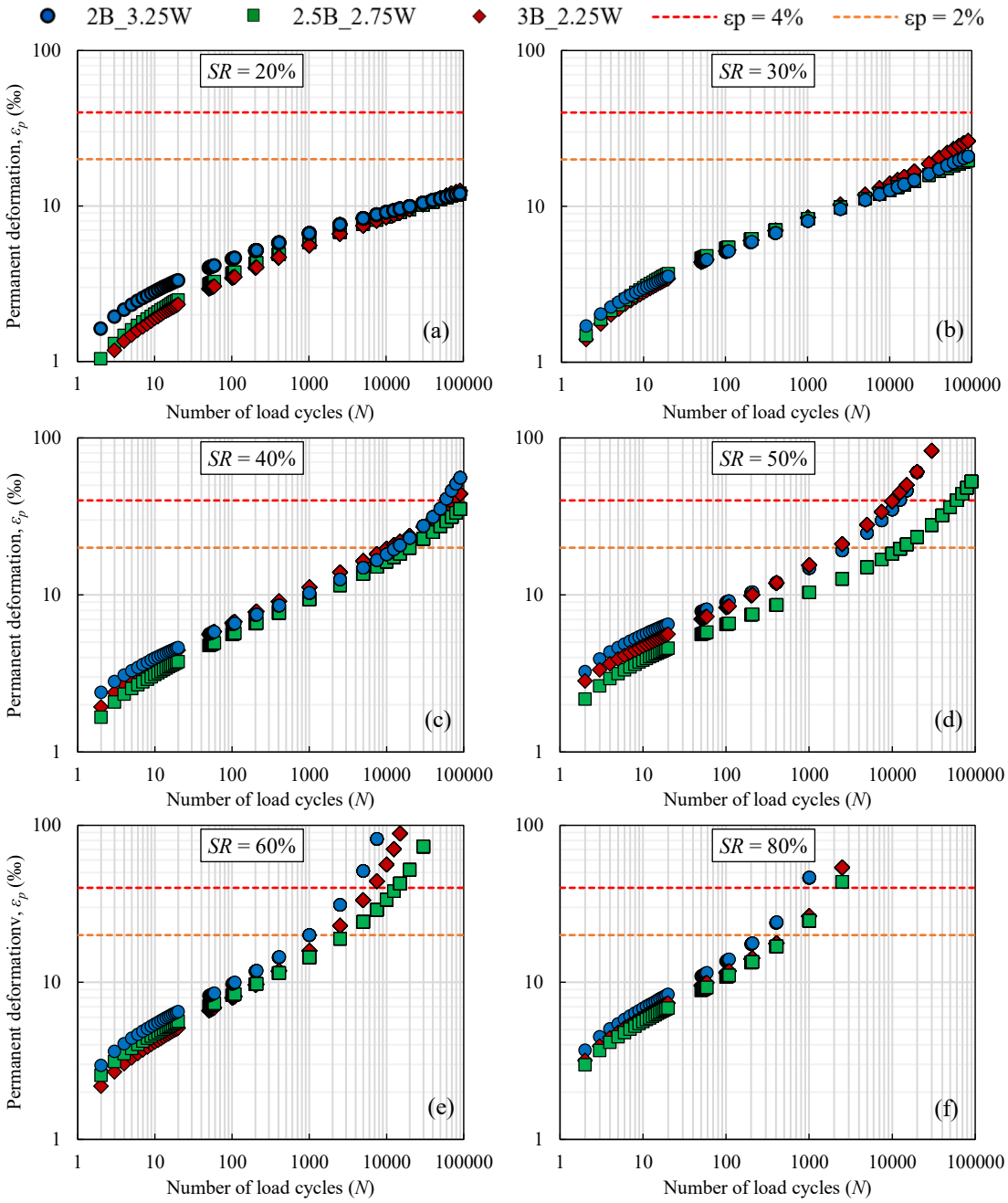

Fig. 11. Comparison of the permanent deformation curves of the three mixtures studied for the same SRs.

Permanent deformation values greater than 2.00% are considered excessive according to the followed standard [39]: However, other researchers who used triaxial tests to study the permanent deformation of the BSM considered the limit of excessive deformation to be 4.00% [9,10]. In the present study, both limits were considered to determine these differences.

When the mixtures were subjected to RLPD triaxial testing with 20% *SR* (Fig. 11a), the strains were usually stabilised before reaching the tertiary stage in any case. It is worth noting that, in Fig. 11a, the permanent deformation at which the three mixtures stabilised was very similar, between 1.20 and 1.25%. As shown in Fig. 11b, when the *SR* was increased to 30%, the differences between the mixtures became more noticeable. Mixtures 2B_3.25 W and 2.5B_2.75 W exhibited similar deformations after 90,000 cycles, both close to 2.00%, at the limit considered. However, mixture 3B_2.25 W experienced a slightly higher deformation after 90,000 cycles, approximately 2.63%, surpassing the first considered deformation limit. As mentioned previously, 20% was considered to be the critical *SR* of this mixture (Table 5). A clear stabilisation of the deformation was not achieved, resulting in higher deformations than those of the other two mixes after completing all the cycles.

For the remaining cases in Fig. 11, because the critical *SRs* were already exceeded in all cases, the deformations surpassed the limit of 2.00% before 90,000 cycles. Indeed, with increasing *SR*, such excessive deformations occurred before for a lower number of cycles in all cases. However, it is imperative to highlight that mixture 2.5B_2.75 W exhibited a better permanent deformation response than the other mixtures. Even considering $SR = 40\%$, it is evident that the mixture 2.5_2.75 W is the only one that continually strain below the 4.00% limit after 90,000 cycles. In all cases, when the *SR* was higher than the critical value, the deformation curves entered the tertiary phase (Fig. 11). However, mixture 2.5B_2.75 W required a higher *N* to reach the same deformations as the rest of the mixtures.

The RLPD triaxial tests were performed on cured specimens with the same volumetric properties as those listed in Table 4, with similar air void contents in all the mixtures. Therefore, the key differences between the mixtures were the proportions of binder, which was the reason for the differences in the results. A high *BC* provides greater flexibility while worsening the behaviour under permanent deformation (mixture 3B_2.25 W). Jenkins et al. reported the same conclusion in their studies [9]. Meanwhile, a low *BC* provided greater internal friction, but in cases of high *SR*, creep occurred earlier (mixture 2B_3.25 W). The *BC* of 2.50% proved to be the best in terms of permanent deformation response. Moreover, it was the one with the best results in terms of resilient modulus and evolution with curing time in previous investigations [16].

It should be noted that RLPD triaxial tests are particularly time-consuming, and given the volume of dosages and SRs studied, it was practically not feasible to perform replicate tests to obtain average results. Each line in the graphs in Figs. 10 and 11 represents the test results for one specimen. The fact that these lines of permanent deformation were fairly parallel indicates a certain degree of accuracy in the results and conclusions. However, it is planned to continue this line of research and verify the repeatability of the results.

5.3. Computational predictive models of permanent deformation

Both Paute's and Huurman's models were fitted to the permanent deformation results obtained from RLPD triaxial tests using Excel's optimisation solver function and minimising the squared errors. Paute's model parameters for each mixture (*a, b,* and *B*) are presented in Table 6. Also indicated in the same Table 6 are the *p* and *q* parameters of the stress state and the *m* and *s* parameters obtained from the failure lines of the cured mixes (Fig. 6), all of them used in the model. Lastly, the coefficient of determination R^2 was used to determine the goodness of fit for each case.

Interestingly, during the adjustment of Paute's model, there were some problems with the stress-dependent term, *A* (8). For higher *SRs*, the denominator term $a - b \cdot \frac{q}{p+p^*}$ eventually changes its sign, causing the sign of the predicted deformation to change as well, making it difficult to fit the overall behaviour of the material. This was considered to be one of the reasons why there was no clear trend when the differences between the parameters obtained for the different mixtures was analysed.

The fitted parameters of Huurman's model (*A, B, C,* and *D*) and the coefficient of determination R^2 are listed in Table 7 for each *SR*.

The second summand of Huurman's model (9) (the exponential term) predicts the deformation once the tertiary stage of creep is reached. Thus, it is logical to see that parameters *C* and *D* for the lowest *SR* were practically zero and increased with increasing *SR* for each mixture. Parameter *A* primarily influences the prediction of the starting point of deformation; therefore, this parameter had a tendency to slightly increase with *SR*, similar to the measured deformations. The parameter *B* is responsible for the slope of the curve. As mentioned previously, the permanent deformation curves obtained for each mixture were parallel for different *SRs* during the steady-state stage (Fig. 10). Accordingly, the increase in parameter *B* with *SR* was smaller than that of parameter *A*, resulting *in B* being a significantly more stable

Table 6
Fitted Paute's parameters (a, b, B) as a function of the stress state (p, q, m, s), from the results at the different SRs of the studied mixtures.

Stress ratio (%)	p	q	m	s	a	b	B	R^2
2B_3.25W								
20	175.15	375.44	1.8208	639.71	−367.330	−202.530	−0.233	98.34%
30	237.72	563.16						99.93%
40	300.29	750.88						95.00%
50	362.87	938.60						88.95%
60	425.44	1126.32						86.52%
80	550.59	1501.76						94.25%
2.5B_2.75W								
20	144.25	282.76	1.233	770.70	−1009.347	−847.506	−0.451	93.28%
30	191.38	424.14						96.59%
40	238.51	565.52						99.81%
50	285.64	706.91						98.08%
60	332.76	848.29						94.65%
80	427.02	1131.05						97.92%
3B_2.25W								
20	148.46	295.39	1.094	882.17	−212.310	−189.050	−0.323	98.21%
30	197.69	443.08						99.89%
40	246.92	590.77						98.54%
50	296.16	738.47						92.71%
60	345.39	886.16						89.52%
80	443.85	1181.54						92.84%

Table 7
Fitted Huurman's parameters (A, B, C, D) as a function of the SR for the studied mixtures.

Stress ratio (%)	A	B	C	D	R^2
2B_3.25W					
20	0.005755	0.144539	0.002434	0.000510	99.06%
30	0.008644	0.176183	0.003125	0.005541	99.93%
40	0.011537	0.202753	0.003731	0.030092	99.80%
50	0.014432	0.226093	0.004281	0.111810	99.43%
60	0.017329	0.247143	0.004790	0.326756	99.63%
80	0.023129	0.284415	0.005719	1.774660	99.52%
2.5B_2.75W					
20	0.005093	0.210172	0.001730	0.000023	98.93%
30	0.007389	0.226598	0.002731	0.000431	99.71%
40	0.009622	0.239025	0.003777	0.003499	98.55%
50	0.011809	0.249132	0.004857	0.017757	99.43%
60	0.013960	0.257706	0.005964	0.066950	99.58%
80	0.018179	0.271839	0.008248	0.543533	99.65%
3B_2.25W					
20	0.005738	0.135982	0.000269	0.001100	99.94%
30	0.008907	0.203956	0.000445	0.007948	99.03%
40	0.012168	0.271926	0.000636	0.032332	99.81%
50	0.015499	0.339891	0.000839	0.096012	98.46%
60	0.018888	0.407854	0.001052	0.233634	99.44%
80	0.025804	0.543773	0.001503	0.950463	99.47%

parameter within each mixture.

Considering its applicability for the simulation of material behaviour in numerical models, the characteristic parameters of each mixture (a_1, a_2, b_1, b_2, c_1, c_2, d_1, and d_2) adjusted in Huurman's model are presented in Table 8.

As an example, Fig. 12 illustrates the graph of the two predictive models adjusted to the permanent deformation of mixture 2.5B_2.75 W, which proved to have the best permanent deformation behaviour. Since Paute's model only predicts deformation based on the measured deformation on cycle number 100, it is represented starting from this cycle. It was observed that the fitting, particularly in the tertiary stage, was much better using Huurman's model, defining the increasing slope of the deformation for high SR accurately owing to the exponential term.

Fig. 13 presents graphs related to the results of the measured deformations from the RLPD triaxial tests versus the predicted deformations obtained from the fitted models. Similar to the previous figures, the colours used in the markers indicate the *SRs*, and the diagonal line corresponds to the complete equality between the measured and predicted values. Fig. 13a shows that the Huurman model provided a good adjustment for all *SRs*, even for high deformations. However, in the case of the Paute model (Fig. 13b), for higher deformations, the model tended to underestimate the actual deformation values. As previously discussed, Paute's model does not accurately estimate the high deformations when the material reaches the tertiary stage because it does not contain an exponential term like in Huurman's model. Therefore, the Huurman model, best predicts the deformation of the CIR mixtures studied at all stress levels. Therefore, it is recommended for this type of analysis in BSM. By combining these predictive models with FEM software, it is possible to simulate the behaviour of pavements with CIR mixtures layers. As an additional result, the authors are currently performing such simulations with the adjusted parameters.

6. Conclusions

In this study, triaxial tests were performed to mechanically characterise three cold recycled mixtures containing 100% RAP and different proportions of bituminous emulsion and water. Binder contents of 2.00%, 2.50%, and 3.00% were selected, and a gyratory compactor was used to prepare the specimens.

Monotonic triaxial tests to failure were performed on the cured and uncured specimens at different confining pressures (25, 50, 100, and 200 kPa). From these results, the Mohr–Coulomb diagrams, failure envelopes, and shear parameters (cohesion and internal friction angle) were determined. Repeated load permanent deformation (RLPD) triaxial tests were performed with different stress ratios (*SR*), obtaining the cumulative permanent deformation curves and the critical *SRs* in each case. Based on the results of the RLPD triaxial tests, two mechanistic–empirical (ME) prediction models were adjusted. With the adjusted parameters of these models, it is possible to perform numerical simulations of pavement behaviour assuming the realisation of a CIR, which is planned for future research.

The main conclusions drawn from the results of the study are as follows:

From the monotonic triaxial test

(1) The failure lines and shear parameters of the uncured mixtures did not exhibit significant differences.
(2) In cured mixtures, the effect of the binder is more decisive. The cohesion increased in all cases by more than twice the value obtained without curing. A higher binder content provided greater cohesion. However, the differences between the mixtures were not very high.

After curing, the angle of internal friction increased slightly in the mix with less binder content. However, the effect was detrimental for mixtures with a higher binder content, acting as a lubricant and reducing the internal friction between the aggregates.

From the RLPD triaxial tests

(3) Mixtures prepared with 2.00% and 2.50% *BC* presented a critical *SR* above 30%, while in the mix with 3.00% *BC*, it was lower (approximately 20 %). If these critical *SRs* (shakedown limits) are exceeded in the CRM layer, the pavement section is considered to fail by rutting.
(4) Mixtures prepared with 2.50% *BC* required a greater number of cycles to reach the tertiary stage than the other mixtures studied. This mixture exhibited a lower permanent deformation. The mix with 2.00% *BC* exhibited the greatest deformation, even at low cycles. Meanwhile, the mixture with 3.00% *BC* did not stabilise the permanent deformations for high cycles.

Table 8
Parameters relating Huurman's model parameters (A, B, C, D) to the stress ratio.

	a_1	a_2	b_1	b_2	c_1	c_2	d_1	d_2
2B_3.25W	0.028933	1.003429	0.317155	0.488271	0.006561	0.616090	6.593879	5.882011
2.5B_2.75W	0.022310	0.917860	0.283333	0.185589	0.010606	1.126797	2.758488	7.279381
3B_2.25W	0.032869	1.084525	0.679685	0.999792	0.001982	1.240646	2.822416	4.877576

The model proposed by Francken in 1977 [26] was modified by researchers in subsequent years [34–37]. This model comprises two distinguished summands. The first one is analogous to the classical power model, which can predict the permanent deformation in the first and second stages, and a second exponential term is used to better adjust the deformation shape corresponding to the tertiary stage. Huurman [34] related parameters *A, B, C,* and *D* to the major principal stresses. Van Niekerk [35] modified Huurman's model by following the same approach, which makes its parameters a function of the deviatoric stress, σ_d, and stress ratio, and independent of the confinement pressure, σ_3. Once the model has been adjusted, stress dependence on only *SR* makes the model application particularly versatile.
BC, binder content; EC, emulsion content; AWC, added water content; OFC, optimum fluid content; ρ_m, maximum specific gravity.

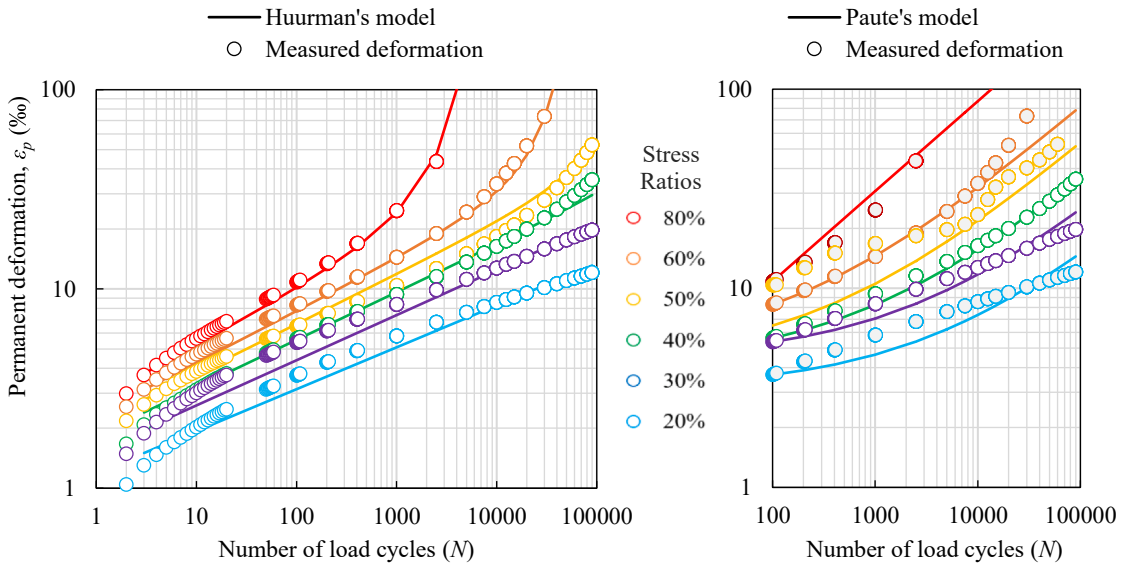

Fig. 12. Huurman's and Paute's predictive models plotted together with the measured permanent deformation of the 2.5B_2.75 W mixture.

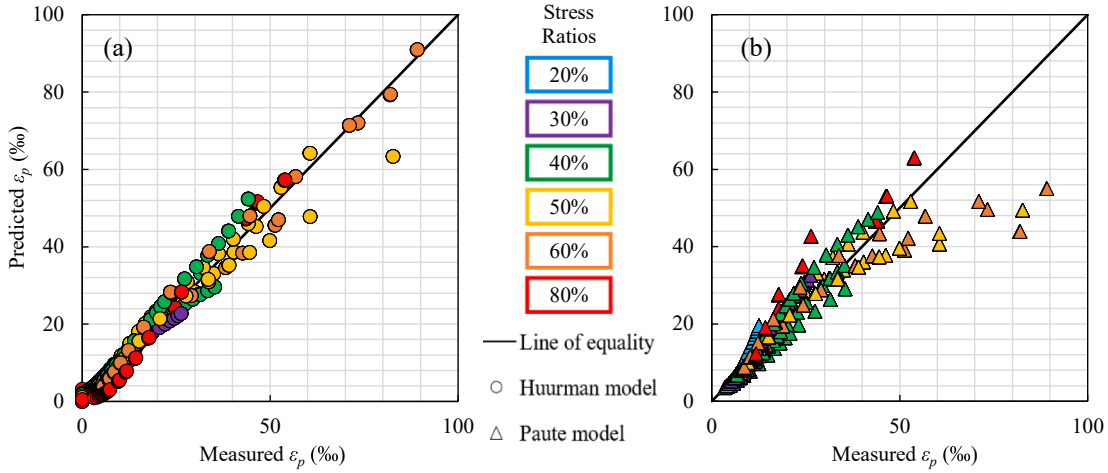

Fig. 13. Predicted versus measured permanent deformation: (a) Huurman's model; (b) Paute's model.

(5) Paute's model fitted the deformations well for low-load cycles and low deformations within the primary and secondary stages. When higher deformations were reached (tertiary stage), the measured results were underestimated.

Huurman's model proved to be the model that best fit the permanent deformation of the mixes studied. It indicated decent adjustment even in the tertiary stage owing to the exponential term included in the model.

In general, during the design of a mixture and the selection of its optimum dosage, the type of stress to which the pavement will be subjected must be considered. When the mixes were stressed to failure rapidly (monotonic triaxial), excess bitumen was found to be detrimental by reducing internal friction. However, the intermediate binder dosage yielded the best results when the response to permanent deformation was evaluated. Generally, a large amount of binder produces soft mixtures that can be deformed more easily. However, lower binder contents produce mixtures with more internal friction but with less flexibility, resulting in creep when the stress ratio increases. Therefore, it is important to gain a good understanding of cold paving technologies, particularly the design of cold in-place recycled mixtures is a fundamental topic that warrants further analysis. Accordingly, it is expected to be addressed in more detail in future research.

Declaration of Competing Interest

The authors declare that they have no known competing financial interests or personal relationships that could have appeared to influence the work reported in this paper.

Acknowledgements

The authors would like to acknowledge the funding for the project BIA2016-80317-R/AEI/10.13039/501100011033 from the Spanish Ministry of Science and Innovation, with an associated pre-doctoral scholarship for the training of research workers (FPI) BES-2017-079633. The authors would also like to express their sincere gratitude to ARIAS INFRAESTRUCTURAS and ECOASFALT for their generous donation of RAP and bitumen emulsion, respectively, for the present research. An special acknowledgement to the Universidade da Coruña/CISUG for funding Elsevier's open access charge. And finally, particular gratitude to N. Pérez-Barge and J. del Valle-Corte for their help in the laboratory work.

References

[1] A.J. Puppala, S. Saride, S. Chomtid, Experimental and modeling studies of permanent strains of subgrade soils, J. Geotech. Geoenviron. Eng. 135 (10) (2009) 1379–1389, https://doi.org/10.1061/(ASCE)GT.1943-5606.0000163.

[2] S. Jain, B. Singh, Cold mix asphalt: An overview, J. Cleaner Prod. 280 (2021), 124378, https://doi.org/10.1016/j.jclepro.2020.124378.

[3] F. Xiao, S. Yao, J. Wang, X. Li, S. Amirkhanian, A literature review on cold recycling technology of asphalt pavement, Constr. Build. Mater. 180 (2018) 579–604, https://doi.org/10.1016/j.conbuildmat.2018.06.006.

[4] T. Chen, T. Ma, X. Huang, S. Ma, F. Tang, S. Wu, Microstructure of synthetic composite interfaces and verification of mixing order in cold-recycled asphalt emulsion mixture, Journal of Cleaner Production 263 (2020) 121467.

[5] J. Zhu, T. Ma, Z. Dong, Evaluation of optimum mixing conditions for rubberized asphalt mixture containing reclaimed asphalt pavement, Constr. Build. Mater. 234 (2020), 117426, https://doi.org/10.1016/j.conbuildmat.2019.117426.

[6] N. Thom, A. Dawson, Sustainable road design: promoting recycling and non-conventional materials, Sustainability 11 (21) (2019) 6106, https://doi.org/10.3390/su11216106.

[7] A. Pakes, T. Edil, M. Sanger, R. Olley, T. Klink, Environmental benefits of cold-in-place recycling, Transp. Res. Rec. 2672 (24) (2018) 11–19, https://doi.org/10.1177/0361198118758691.

[8] P. Orosa, A.R. Pasandín, I. Pérez, Assessment of two laboratory design methods for CIR mixtures with bitumen emulsion based on static and gyratory compaction, Constr. Build. Mater. 265 (2020), 120667, https://doi.org/10.1016/j.conbuildmat.2020.120667.

[9] K.J. Jenkins, F.M. Long, L.J. Ebels, Foamed bitumen mixes= shear performance? Int. J. Pavement Eng. 8 (2) (2007) 85–98, https://doi.org/10.1080/10298430601149718.

[10] L.J. Ebels, (2008). Characterisation of material properties and behaviour of cold bituminous mixtures for road pavements (Doctoral dissertation, Stellenbosch: Stellenbosch University).

[11] Southern African Bitumen Association (Sabita). A Guideline for the Design and Construction of Bitumen Emulsion and Foamed Bitumen Stabilised Materials; Technical Guideline: Bitumen Stabilised Materials, 3rd ed.; Southern African Bitumen Association (Sabita): Cape Town, South Africa, 2020; pp. 1–2, 7–8, 36–37.

[12] I. Pérez, L. Medina, B. Gomez-Meijide, P.A. Costa, A.S. Cardoso, Numerical simulation of bitumen emulsion-stabilised base course mixtures with C&D waste aggregates considering nonlinear elastic behaviour, Constr. Build. Mater. 249 (2020), 118696, https://doi.org/10.1016/j.conbuildmat.2020.118696.

[13] J. Tong, T. Ma, K. Shen, H. Zhang, S. Wu, A criterion of asphalt pavement rutting based on the thermal-visco-elastic-plastic model, Int. J. Pavement Eng. 1–11 (2020), https://doi.org/10.1080/10298436.2020.1792470.

[14] B. Gómez-Meijide, I. Pérez, Nonlinear elastic behavior of bitumen emulsion-stabilized materials with C&D waste aggregates, Constr. Build. Mater. 98 (2015) 853–863, https://doi.org/10.1016/j.conbuildmat.2015.07.004.

[15] Z. Čížková, J. Šedina, J. Valentin, D.M. Engels, (2016). Laboratory experience with the application of monotonic triaxial test on the cold recycled asphalt mixes. 6th Eurasphalt & Eurobitume Congress.

[16] P. Orosa, I. Pérez, A.R. Pasandín, Short-term resilient behaviour and its evolution with curing in cold in-place recycled asphalt mixtures, Constr. Build. Mater. 323 (2022), 126559, https://doi.org/10.1016/j.conbuildmat.2022.126559.

[17] M.W. Witczak, Simple performance test for superpave mix design, 465, Transportation Research Board, 2002.

[18] T.W. Lambe, R.V. Whitman, Soil Mechanics, John Wiley & Sons, USA, 1969.

[19] X. Ling, P. Li, F. Zhang, Y. Zhao, Y. Li, L. An, Permanent deformation characteristics of coarse grained subgrade soils under train-induced repeated load, Adv. Mater. Sci. Eng. 2017 (2017) 1–15.

[20] A. Ramos, A.G. Correia, B. Indraratna, T. Ngo, R. Calçada, P.A. Costa, Mechanistic-empirical permanent deformation models: Laboratory testing, modelling and ranking, Transp. Geotech. 23 (2020), 100326, https://doi.org/10.1016/j.trgeo.2020.100326.

[21] S. Werkmeister, R. Numrich, F. Wellner, The development of a permanent deformation design model for unbound granular materials with the shakedown-concept. In Bearing Capacity of Roads, Railways and Airfields, CRC Press, 2002, pp. 1081–1096.

[22] AENOR, Spanish Association for Standardisation and Certification, 2008. UNE–EN 13286–7. Unbound and hydraulically bound mixtures. Part 7: Cyclic load triaxial test for unbound mixtures. Madrid. In Spanish.

[23] J. Qian, H. Lin, X. Gu, J. Xue, Dynamic shakedown limits for flexible pavement with cross-anisotropic materials, Road Mater. Pavement Des. 21 (2) (2018) 310–330, https://doi.org/10.1080/14680629.2018.1491881.

[24] J. Qian, Y. Wang, J. Wang, M. Huang, The influence of traffic moving speed on shakedown limits of flexible pavements, Int. J. Pavement Eng. 20 (2) (2019) 233–244, https://doi.org/10.1080/10298436.2017.1293259.

[25] R.D. Barksdale, (1972, September). Laboratory evaluation of rutting in base course materials. In Presented at the Third International Conference on the Structural Design of Asphalt Pavements, Grosvenor House, Park Lane, London, England, Sept. 11-15, 1972. (Vol. 1, No. Proceeding).

[26] L. Francken, Permanent deformation law of bituminous road mixes in repeated triaxial compression, in: 4th International Conference on the Structural Design of asphalt Pavements, Ann Arbor, Michigan, USA, 1977.

[27] J.L. Paute, P. Jouve, J. Martínez, E. Ragneau, (1988). Modèle de calcul pour le dimensionnement des chaussées souples. Bulletin de liaison des laboratoires des ponts et Chaussées, (156).

[28] J.L. Paute, P. Hornych, J.P. Benaben, Comportement mécanique des graves non traitées, Bulletin de liaison des Laboratoires des Ponts et Chaussées 190 (1994) 27–38.

[29] G.T.H. Sweere, Unbound granular bases for roads, Delft University of Technology, Netherlands, 1990. PhD Thesis.

[30] B. Vuong, (1994). Evaluation of back-calculation and performance models using a full scale granular pavement tested with the accelerated loading facility (alf). In 4th International Conference, Bearing Capacity of Roads and AirfieldsFHWA, U of Minnesota, Army Corps of Engineers, NRC Canada, FAA (Vol. 1).

[31] H. Wolff, A.T. Visser, (1994, November). Incorporating elasto-plasticity in granular layer pavement design. In Proceedings of the Institution of Civil Engineers-Transport (Vol. 105, No. 4, pp. 259-272). Thomas Telford-ICE Virtual Library.

[32] F. Lekarp, (1997). Permanent deformation behaviour of unbound granular materials. Licentiate Thesis. Department of Infrastructure and Planning, Royal Institution of Technology, Stockholm. TRITA-IP FR, (97-20).

[33] F. Lekarp, A. Dawson, Modelling permanent deformation behaviour of unbound granular materials, Constr. Build. Mater. 12 (1) (1998) 9–18, https://doi.org/10.1016/S0950-0618(97)00078-0.

[34] H. Huurman, Permanent deformation in concrete block pavements (Doctoral Dissertation), Delft University of Technology, The Netherlands, 1997.

[35] A.A. Van Niekerk, Mechanical Behavior and Performance of Granular Bases and Sub-Bases in Pavements (Doctoral dissertation), Delft University of Technology, The Netherlands, 2002.

[36] S. Werkmeister, Permanent deformation behaviour of unbound granular materials in pavement construction, Dresden University of Technology, Germany, 2003. PhD thesis.

[37] Arnold G. Rutting of granular pavement. PhD thesis, University Of Nottingham, England, UK; 2004.

[38] AENOR, Spanish Association for Standardisation and Certification, 2015. UNE–EN 12697–2. Bituminous mixtures. Test methods. Part 2: Determination of particle size distribution. Madrid, Spain. In Spanish.

[39] Ministry of Development (2017) Recycling of bituminous pavements and roadways. Circular Order 40/2017. In Spanish.

[40] A. Academy, – TG2. Technical Guideline: Bitumen Stabilised Materials – A Guideline for the Design and Construction of Bitumen Emulsion and Foamed Bitumen Stabilised Materials (TG2), Third Edition. Sabita. (2020).

[41] AENOR, Spanish Association for Standardisation and Certification, 2013. UNE–EN 13808. Bitumen and bituminous binders. Framework for specifying cationic bituminous emulsions. Madrid, Spain. In Spanish.

[42] Ministry of Public Works and Transport, 1990. NLT standards. NLT–164/90. Binder content in bituminous mixtures. Road tests. Directorate General for Roads, 2nd ed. Madrid, Spain. In Spanish.

[43] AENOR, Spanish Association for Standardisation and Certification, 2006. UNE–EN 1097–6. Tests to determine the mechanical and physical properties of aggregates. Part 6: Determination of particle density and water absorption. Madrid, Spain. In Spanish.

[44] AENOR, Spanish Association for Standardisation and Certification, 2015. UNE–EN 1427. Bitumen and bituminous binders. Determination of the softening point. Ring and Ball method. Madrid, Spain. In Spanish.

[45] AENOR, Spanish Association for Standardisation and Certification, 2015. UNE–EN 1426. Bitumen and bituminous binders. Determination of needle penetration. Madrid, Spain. In Spanish.

[46] AENOR, Spanish Association for Standardisation and Certification, 2013. UNE–EN 1429. Bitumen and bituminous binders. Determination of residue on sieving of bituminous emulsions, and determination of storage stability by sieving. Madrid, Spain. In Spanish.

[47] AENOR, Spanish Association for Standardisation and Certification, 1994. UNE–EN 10 103–501–94. Geotechnics. Compaction test. Modified Proctor. Madrid. In Spanish.

[48] AENOR, Spanish Association for Standardisation and Certification, 2008. UNE–EN 12697–31. Bituminous mixtures. Test methods for hot bituminous mixtures. Part 31: Specimen preparation by gyratory compactor. Madrid. In Spanish.

[49] AENOR, Spanish Association for Standardisation and Certification, 2010. UNE–EN 12697–5. Bituminous mixtures. Test methods for hot bituminous mixtures. Part 5: Determination of the maximum density. Madrid. In Spanish.

[50] R. Garba, Permanent deformation properties of asphalt concrete mixtures. Department of Road and Railway Engineering, Ph.D. Dissertation, Norwegian University of Science and Technology NTNU August 2002, Norwegian University of Science and Technology, 2002.

[51] P. Orosa, A.R. Pasandín, I. Pérez, Compaction and volumetric analysis of cold in-place recycled asphalt mixtures prepared using gyratory, static, and impact procedures, Constr. Build. Mater. 296 (2021), 123620, https://doi.org/10.1016/j.conbuildmat.2021.123620.

[52] E. Santagata, G. Chiappinelli, P.P. Riviera, O. Baglieri, Triaxial testing for the short term evaluation of cold-recycled bituminous mixtures, Road Mater. Pavement Des. 11 (1) (2010) 123–147, https://doi.org/10.1080/14680629.2010.9690263.

[53] T. Yun, Y.R. Kim, Viscoelastoplastic modeling of the behavior of hot mix asphalt in compression, KSCE J. Civ. Eng. 17 (6) (2013) 1323–1332, https://doi.org/10.1007/s12205-013-0352-7.

[54] W. Kim, J. Labuz, Resilient modulus and strength of base course with recycled bituminous material, (Technical report) (2007).

[55] T.W. Lambe, R.V. Whitman, Soil mechanics, Vol. 10, John Wiley & Sons, 1991.

[56] I. Pérez, L. Medina, M.G. Romana, Permanent deformation models for a granular material used in road pavements, Constr. Build. Mater. 20 (9) (2006) 790–800, https://doi.org/10.1016/j.conbuildmat.2005.01.050.

[57] I. Pérez, J. Gallego, Rutting prediction of a granular material for base layers of low-traffic roads, Constr. Build. Mater. 24 (3) (2010) 340–345, https://doi.org/10.1016/j.conbuildmat.2009.08.028.
[58] F.M. Long, H.L. Theyse, The engineering, mechanical and durability properties of crushed hornfels treated with emulsified bitumen and of sand treated with emulsified bitumen and foamed bitumen, CSIR Transportek Contract Report CR-2005 (2005) 1.
[59] K.H. Jenkins, Mix Design Considerations for Cold and Half-Warm Bituminous Mixes with Emphasis on Foamed Bitumen (Doctoral dissertation), University of Stellenbosh, South Africa, 2000.